Applied Energy 199 (2017) 1–12

Contents lists available at ScienceDirect

Applied Energy

journal homepage: www.elsevier.com/locate/apenergy

Electro-hydraulic damper for energy harvesting suspension: Modeling, prototyping and experimental validation

Yuxin Zhang [a,b,*], Hong Chen [a,b], Konghui Guo [a], Xinjie Zhang [a], Shengbo Eben Li [c]

[a] State Key Laboratory of Automotive Simulation and Control, Jilin University, Changchun, Jilin 130022, PR China
[b] Department of Control Science and Engineering, Jilin University, Changchun, Jilin 130022, PR China
[c] State Key Laboratory of Automotive Safety and Energy, Tsinghua University, Beijing 100084, PR China

HIGHLIGHTS

- A novel electro-hydraulic energy harvesting damper was proposed for off-road vehicles.
- Unidirectional generator rotation was realized to improve energy harvesting efficiency.
- Asymmetric rebound/compression damping force was obtained for better road-tire contact.
- Damping and regenerative characteristics were studied via simulation and test.
- Large controllable damping range is achieved as the basis to control active suspension.

ARTICLE INFO

Article history:
Received 22 November 2016
Received in revised form 25 April 2017
Accepted 28 April 2017

Keywords:
Energy harvesting
Vehicle suspension
Electro-hydraulic damper
Off-road vehicle

ABSTRACT

This paper presents an electro-hydraulic semi-active damper to harvest the suspension kinetic energy for the purpose of further improving the fuel efficiency of off-road vehicles. This regenerative damper can transform the reciprocating suspension vibration into unidirectional generator rotation, and meanwhile achieve approximately asymmetric rebound/compression damping force in a wide controllable region. The working mechanism of this new damper is first elaborated, and then its dynamic model is mathematically derived based on the first-principle analysis of hydraulic and electric components. A prototyping damper is designed and manufactured, and a series of experimental tests are conducted to demonstrate its effectiveness to generate the damping characteristic and energy harvesting capability.

1. Introduction

Many studies on the low carbon vehicles have been focusing on how to reduce energy consumption as much as possible [1,2]. The most famous efforts in automotive industry include powertrain energy management [3] and braking-energy recovery [4]. The harvesting of suspension energy is a new trial, however, the main challenge is to reduce its influence on vehicle dynamical performances while reducing fuel usage [5]. In the daily usage of a ground vehicle, only 10–16% of fuel energy is used to drive the car to overcome the resistance from road friction and air drag [6]. One major loss is the dissipation of vibration energy by active and/or semi-active suspensions under the excitation of vehicle acceleration and road irregularity, especially for off-road vehicles.

For the off-road vehicles, such as military vehicles and SUVs, the energy harvesting suspension has more potential for the industry application [7]. Zuo et al. [8] suggest that road roughness, tire stiffness, and vehicle driving speed have great influences on the harvesting power potential, and for a middle-sized vehicle, 100–400 W average power is available in the suspensions at 60 mph on B and C class roads. The road tests conducted by Audi AG [9] show that the average recovery power is about 150 W when the passenger car is driven on German roads, 3 W on newly paved highways, and 613 W on the rugged country road. Moreover, the dampers for off-road vehicles need to frequently move fast and at a large stroke to be able to drive off the pavement, which leads to serious temperature-rise in damping oil. This temperature-rise severely affects the vehicle performance and accelerates the failure of damper components [10]. The damping oil temperature rises rapidly, which means that there is a considerable energy dissipation to the surrounding environment, and this dissipated energy also comes from the vehicle's engine power [11].

* Corresponding author at: State Key Laboratory of Automotive Simulation and Control, Jilin University, Changchun, Jilin 130022, PR China.
E-mail addresses: yuxinzhang@jlu.edu.cn (Y. Zhang), chenh@jlu.edu.cn (H. Chen).

http://dx.doi.org/10.1016/j.apenergy.2017.04.085
0306-2619/

The energy harvesting damper is the core of active and semi-active suspensions, which can be categorized into two types: electromagnetic and electro-hydraulic. The electromagnetic regenerative damper mainly contains two components: energy conversion (linear or rotary electric generators) and transmission (from reciprocation to rotation) devices.

The transmission device is used to transmit the reciprocating suspension vibration into rotation for easier energy conversion. The key techniques of transmission device include ball screw, rack-pinion, hydraulic transformation system and link mechanism, etc. Zuo and Scully design a retrofit regenerative damper for compact space deployment, in which a four-phase linear generator with high permeable magnetic loops is used to directly harvest reciprocating vibration [12]. The general layout of linear motor electromagnetic regenerative damper is shown in Fig. 1(a).

Song et al. patented a regenerative suspension system based on the rotary electromagnetic motor and ball screw mechanism, which can switch between passive mode and semi-active mode [13]. Kawamoto et al. [14] and Singal et al. [15] analyzed the relationship between suspension damping performance and energy consumption of this kind of regenerative suspension, and achieved zero-energy semi-active damping adjustment via Skyhook adaptive control algorithm. The simplest layout of such electromagnetic regenerative damper is shown in Fig. 1(b). Li and Zuo [16,17] designed a regenerative damper based on the rotary electromagnetic motor and rack-pinion mechanism, which can switch reciprocating suspension vibration movement into unidirectional generator rotation via a mechanical motion rectifier (MMR), and adjust the suspension damping coefficient by changing external load connected with the generator. The prototype test results show that the power regenerative efficiency of this regenerative damper can reach to 60% under high frequency excitation. Zhang et al. [18] proposed a novel high-efficiency energy regenerative damper using rack-pinion mechanism and supercapacitors, and then this damper is applied to extend the battery endurance of an electric vehicle (EV). The general layout of rack-pinion regenerative damper is shown in Fig. 1(c).

Self-powered system design combined with electrorheological (ER) or magnetorheological (MR) dampers is another hot topic. Choi et al. [19] set a rack-pinion mechanism outside of the outer cylinder of an ER damper, which can change the linear reciprocating vibration into generator rotation, and then the power outputted from the generator can be used as power supply for the sensing system of ER suspension. Sapinski [20,21] paralleled an electromagnetic induction device (EMI) with a MR damper, and the EMI harvests suspension vibration into electricity which can be used to power the control and sensor system of the MR suspension.

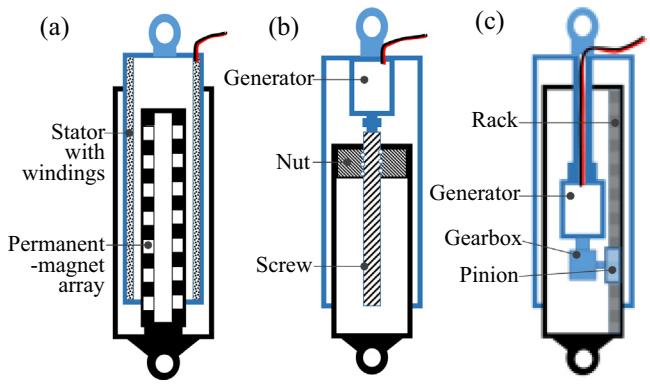

Fig. 1. The general layout of different electromagnetic regenerative dampers. (a) Linear motor, (b) ball screw, and (c) rack-pinion.

The electro-hydraulic regenerative damper also has many different layouts. Stansbury et al. [22] disclosed an electro-hydraulic regenerative damper, whose hydraulic circuit can switch reciprocating piston vibration into hydraulic energy, and then drive the hydraulic motor and generator to rotate, in order to convert the hydraulic energy into electricity. Due to the randomness of the uneven road excitation, the oil flow direction will be switched frequently, which not only reduces the working reliability of the system, but also greatly decreases the energy efficiency of the generator.

Guo et al. designed a pumping electro-hydraulic regenerative damper [23] and an interconnected active regenerative suspension system [24]. After analyzing the relationship between regenerative damper and vehicle fuel efficiency [25], the results show that the off-road vehicles and heavy trucks have more potential to improve the fuel economy via the regenerative damper.

Electromagnetic regenerative damper has a relative low load carrying capacity, therefore it is more suitable for minivans and passenger cars etc. Electro-hydraulic damper can provide a higher damping force which is usually required by off-road vehicles. Therefore, it is more practical to study the electro-hydraulic energy harvesting suspension for off-road vehicles, heavy trucks, mining vehicles, military vehicles and engineering vehicles, which have large weight and poor road conditions.

This paper presents an electro-hydraulic energy harvesting damper, which has following advantages: (1) transform the reciprocating shift of the suspension vibration into unidirectional generator rotation which can improve energy converting efficiency, (2) realize approximately asymmetry rebound/compression damping force which is useful to improve vehicle handling, and (3) achieve relatively large controllable range of damping force to make it possible to be used in active/semi-active suspension.

The rest of this paper is organized as follows: In Section 2, an electro-hydraulic energy harvesting damper design is proposed and its mathematical model is introduced. The prototype design and test setup are given in Section 3. Simulation and experimental verification results and discussions of the oil temperature-rise, passive damping, damping force controllable and regenerative characteristics are given in Section 4. This is followed by the concluding remarks and future issues in the final section.

2. Damper design and modeling

Based on the analysis and summary of existing energy harvesting suspension systems, their general configuration is illustrated in Fig. 2. The actuator and energy harvesting module (can be collectively referred as regenerative damper) are the core parts of this kind of suspension system, which can transform suspension reciprocating mechanical vibration into recoverable electricity. Due to the random road excitation, the output voltage of above regenerative damper usually fluctuates in a wide range. The charge management module in Fig. 2 is used to narrow the range of fluctuating voltage, thus efficiently charging the battery pack. By collecting the suspension feedback signals, the controller can regulate the charge management module in real time, and improve the ride comfort and fuel efficiency.

2.1. Design

Three pumping electro-hydraulic regenerative dampers (e.g., mono-tube [23], twin-tube [24] and integrated mono-tube [26]) were designed. Each of them has its own advantages and disadvantages, and is applicable to different vehicle requirements and installation conditions. However, they share similar design requirements: (1) improve the generator efficiency and reliability

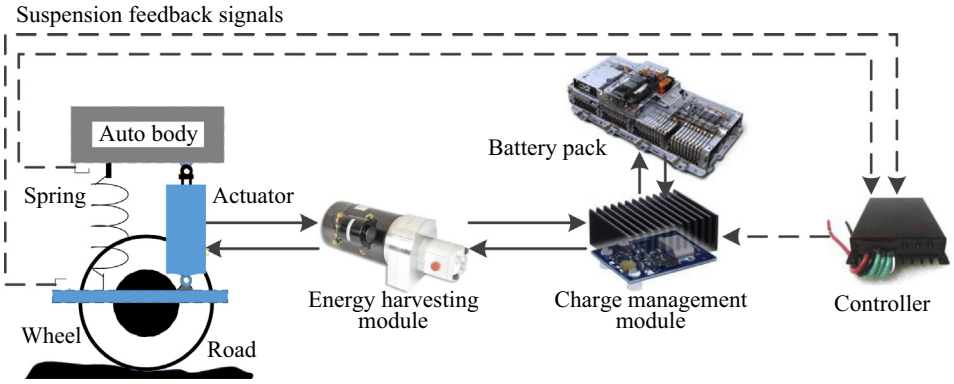

Fig. 2. General configuration of regenerative suspension systems.

by transforming the reciprocating suspension vibration into one-way oil flow and one-way rotation of hydraulic motor and generator; (2) achieve asymmetry rebound/compression damping forces required by vehicle suspension performance via designing the hydraulic circuit; and (3) increase the controllable range of damping force to provide a good basis for future semi-active or active suspension control.

This paper focuses on the design and experimental study of the twin-tube pumping regenerative damper, which is shown in Fig. 3. There is an inner tube between the pressure tube and reserve tube of the actuator, which has a circulation hole to connect the upper cavity and the hydraulic motor inlet; the hydraulic motor outlet is connected to the reserve cavity via oil pipe. In order to achieve one-way oil flow, there is one check valve arranged on the piston and one on the base valve, respectively, which can be both opened upwards.

The operating process of this scheme is illustrated in Fig. 4. When the piston rod of the actuator is moving upward (rebound), the check valve 1 closes and check valve 2 opens, the high-pressure oil flow in upper cavity flows into motor inlet through the middle cavity and pipe and drives the motor to rotate; and then the low-pressure oil flows out of motor outlet and returns to the reserve cavity and finally goes back into the lower cavity through check valve 2. Due to the extract of the piston rod, the whole volume of the actuator is enlarged, therefore, the high-pressure nitrogen will press some oil in the reserve cavity into the lower cavity thus

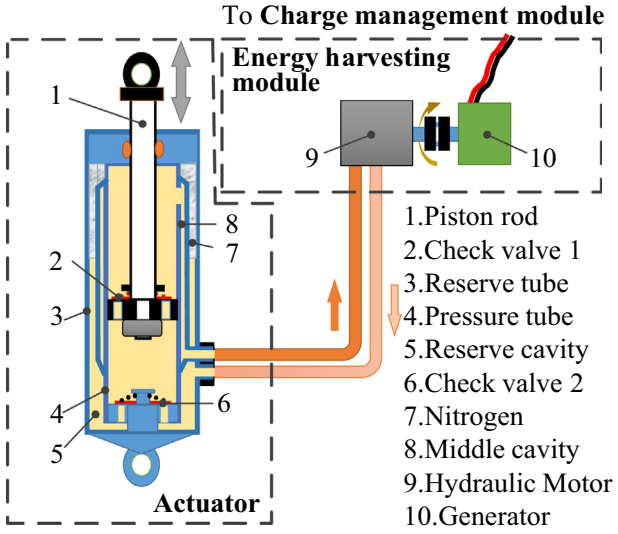

Fig. 3. Twin-tube pumping regenerative damper.

compensate the oil loss. When the piston rod is moving downward (compression), see Fig. 4 (b), the check valve 1 opens and check valve 2 closes, the high-pressure oil in the lower cavity flows into upper cavity through check valve 1. Due to the insertion of the piston rod, the volume of the actuator is decreased, therefore, the high-pressure oil will continue to flow into motor inlet through middle cavity and oil pipe, and finally drive the motor to rotate. The low-pressure oil from the outlet will flow back into the reserve cavity and compress the nitrogen.

It is observed that, no matter the piston rod is moving upward or downward, the oil flow direction and the motor rotation direction are not changed in this scheme, which can achieve a unidirectional rotation of the generator.

2.2. Modeling

This section will analyze and explain the design scheme to obtain the principle schematic diagram, and then build the dynamic model by calculating the controllable and passive damping forces, which can provide a theoretical basis for the performance analysis.

2.2.1. Principle analysis

The principle schematic diagram is shown in Fig. 5, where A is the actuator, B the energy harvesting module, C the charge management module, 1 the equivalent hydraulic cylinder, 2 the check valve 1, 3 the check valve 2, 4 the accumulator (equivalent to the high-pressure nitrogen), 5 the hydraulic motor, 6 the ideal generator, 7 the internal resistance of the generator, and 8 the internal inductance of the generator.

The total damping force of the regenerative damper can be divided into two parts:

(1) Equivalent controllable damping force, $F_{semi\text{-}active}$, which is produced by the back EMF of the generator, it can be adjusted by the equivalent external load of the charge management module. The equivalent controllable damping force is a basis to achieve the active of semi-active suspension control;
(2) Passive damping force, $F_{passive}$, which is produced by the motor rotating resistance, actuator orifices, oil pipelines and check valves, this part of damping force is not controllable and is also the reason of damping oil temperature-rise.

2.2.2. Motor flow analysis

According to the working principle of the pumping damper, the volumetric flow rate of the oil flowing through the hydraulic motor is different during the rebound and compression strokes. The

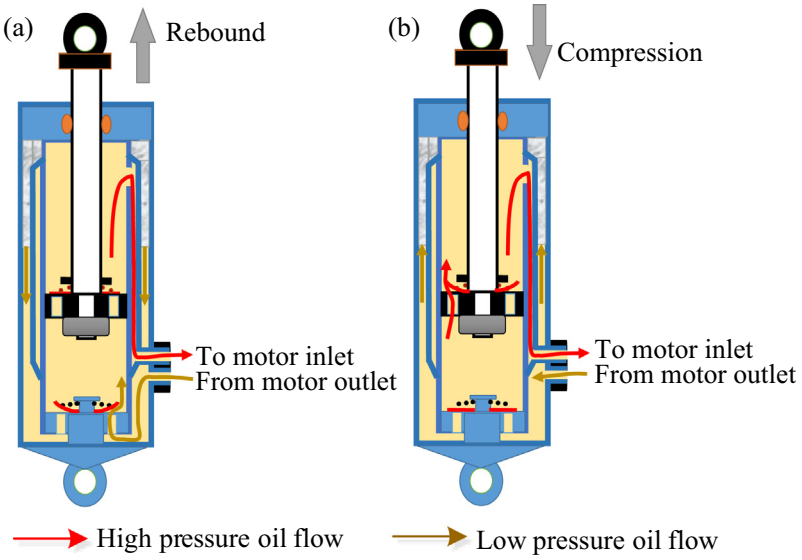

Fig. 4. Working process of twin-tube pumping regenerative damper.

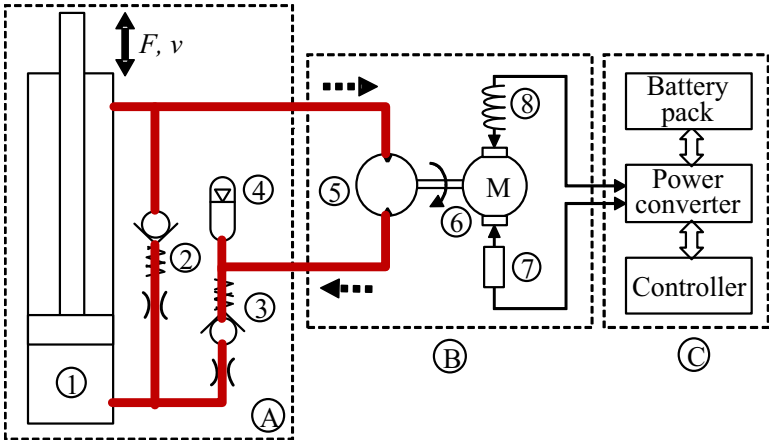

Fig. 5. Schematic diagram of pumping regenerative damper.

motor flow analysis of the pumping regenerative damper is illustrated in Fig. 6.

During the rebound stroke, the volume of oil flows into the motor is equivalent to piston ring section area (piston section area minus piston rod section area) multiplied by rod velocity; while during the compression stroke, the oil flow is equivalent to the piston rod section area multiplied by rod velocity. This difference indicates the asymmetry rebound/compression damping force, which will be further demonstrated in Section 4. During the rebound stroke, the oil flows through each component are:

$$\begin{cases} Q_{pipe} = Q_{motor} = A_c v(t) \\ Q_{valve\_1} = 0 \\ Q_{valve\_2} = A_g v(t) \end{cases}, \quad v(t) \geqslant 0 \tag{1}$$

During the compression stroke, the oil flows through each component are:

$$\begin{cases} Q_{valve\_1} = |A_g v(t)| \\ Q_{pipe} = Q_{motor} = |A_r v(t)|, \\ Q_{valve\_2} = 0 \end{cases} \quad v(t) \leqslant 0 \tag{2}$$

where Q_{pipe}, Q_{motor}, Q_{valve_1} and Q_{valve_2} are oil volumetric flow rate (mm^3/s) through the pipe, motor, check valve 1 and check valve 2, respectively, A_c is the piston ring section area (mm^2), $A_c = A_g - A_r = \pi(D^2 - d_{rod}^2)/4$, $v(t)$ is the rod velocity (mm/s), A_g is the piston section area (mm^2), $A_g = \pi D^2/4$, A_r is the piston rod section area (mm^2), $A_r = \pi d_{rod}^2/4$, D and d_{rod} are the diameter (mm) of piston and piston rod, respectively.

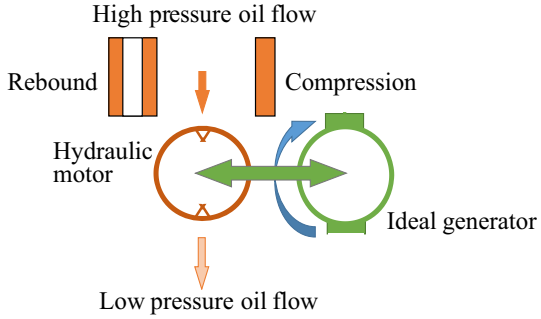

Fig. 6. Motor flow analysis of pumping regenerative damper.

2.2.3. Controllable damping force model

In order to facilitate the analysis and modeling process, the generator is broken into an ideal generator, an internal resistance and an internal inductance; the charge management module is equivalent to an external load, as shown in Fig. 7. Through analyzing the relationship between the pressure and volumetric flow rate of the hydraulic motor and the working characteristics of the generator, the expression of the equivalent controllable damping force $F_{semi\text{-}active}$ and regenerative power can be finally established.The relationship between motor rotation speed ω_{pump} (rad/s) and output torque T_{motor} (N·m) can be expressed as:

$$\begin{cases} \omega_{motor} = \frac{2\pi Q_{motor}}{q}\eta_v \\ T_{motor} = \frac{\Delta P_{motor} q}{2\pi}\eta_m \end{cases} \tag{3}$$

where q is the motor displacement (cc), ΔP_{motor} is the pressure difference of the motor inlet and outlet (Pa), η_v and η_m are the volumetric and mechanical efficiency, respectively.

The output voltage U_{emf} (V) and input torque $T_{generator}$ (N·m) of the generator can be expressed as:

$$\begin{cases} U_{emf} = k_e \omega_{generator} \\ T_{generator} = J_g \frac{d\omega}{dt} + k_t I \end{cases} \tag{4}$$

where $\omega_{generator}$ is the input rotation speed (rad/s) of the generator, k_e and k_t are the EMF constant and torque constant of the generator, respectively, J_g is the moment of inertia (kg·m^2) of the generator rotor, I is the output current (A) of the generator.

Based on the equivalent controllable damping force model and Kirchhoff's Voltage Law, we have:

$$U_{emf} - L_{in}\frac{dI}{dt} - I(R_{in} + R_{ex}) = 0 \tag{5}$$

where L_{in} and R_{in} are the internal inductance (F) and resistance (Ω) of the generator, respectively, the generator internal inductance can be neglected generally; R_{ex} is the external load (Ω) of the generator.

Since the generator and motor are linked together by a shaft coupling, we have:

$$\begin{cases} \omega_{motor} = \omega_{generator} \\ T_{motor} = T_{generator} \end{cases} \tag{6}$$

The relationship between pressure difference ΔP_{motor} and volumetric flow rate Q_{motor} of the motor can be obtained by combining Eqs. (3)(6):

$$\Delta P_{motor} = \frac{4\pi^2 J_g \eta_v}{q^2 \eta_m}\dot{Q}_{motor} + \frac{4\pi^2 k_t k_e \eta_v}{q^2 \eta_m (R_{in} + R_{ex})} Q_{motor} \tag{7}$$

From Eq. (7), we can see that when external load R_{ex} is infinite (e.g. the generator output is open circuit), the motor is working as a passive damping. Therefore, the second term of the right side of Eq. (7) is the controllable pressure difference $\Delta P_{motor,controllable}$ of motor which can be adjusted by the external load R_{ex}:

$$\Delta P_{motor,controllable} = \frac{4\pi^2 k_t k_e \eta_v}{q^2 \eta_m (R_{in} + R_{ex})} Q_{motor} = k_{motor,controllable} Q_{motor} \tag{8}$$

where $k_{motor,controllable}$ is the controllable impedance of the energy harvesting module, which is subject to motor displacement, volumetric efficiency, mechanical efficiency, and generator characteristics. Therefore, the upper pressure $P_{up,controllable}$ and lower pressure $P_{down,controllable}$ of the actuator can be expressed as:

$$\begin{cases} P_{up,controllable} = \Delta P_{motor,controllable} \\ P_{down,controllable} = 0 \end{cases}, \quad v(t) \geqslant 0 \tag{9}$$

$$\begin{cases} P_{up,controllable} = \Delta P_{motor,controllable} \\ P_{down,controllable} = \Delta P_{motor,controllable} \end{cases}, \quad v(t) \leqslant 0 \tag{10}$$

The controllable damping force $F_{semi\text{-}active}$ of the regenerative damper can be obtained by solving Eqs. (1), (2), (9) and (10):

$$\begin{aligned} F_{semi-active} &= A_c P_{up,controllable} - A P_{down,controllable} \\ &= \begin{cases} \frac{\pi^3 k_t k_e \eta_v (D^2 - d_{rod}^2)^2 v(t)}{q^2 \eta_m (R_{in} + R_{ex})}, & v(t) \geqslant 0 \\ -\frac{\pi^3 k_t k_e \eta_v d_{rod}^4 v(t)}{q^2 \eta_m (R_{in} + R_{ex})}, & v(t) \leqslant 0 \end{cases} \end{aligned} \tag{11}$$

The output current I of the generator can be obtained by solving Eqs. (4)(6):

$$\begin{aligned} I &= \frac{2\pi k_e \eta_v}{q(R_{in} + R_{ex})} Q_{motor} \\ &= \begin{cases} \frac{\pi^2 k_e \eta_v (D^2 - d_{rod}^2)}{2q(R_{in} + R_{ex})} v(t), & v(t) \geqslant 0 \\ \frac{\pi^2 k_e \eta_v d_{rod}^2}{2q(R_{in} + R_{ex})} |v(t)|, & v(t) \leqslant 0 \end{cases} \end{aligned} \tag{12}$$

Therefore, the regenerative power $P_{regenerato}$ of this damper can be expressed as:

$$\begin{aligned} P_{regenerative} &= I^2 R_{ex} \\ &= \begin{cases} \frac{\pi^4 k_e^2 \eta_v^2 (D^2 - d_{rod}^2)^2 R_{ex}}{4q^2 (R_{in} + R_{ex})^2} v^2(t), & v(t) \geqslant 0 \\ \frac{\pi^4 k_e^2 \eta_v^2 d_{rod}^4 R_{ex}}{4q^2 (R_{in} + R_{ex})^2} v^2(t), & v(t) \leqslant 0 \end{cases} \end{aligned} \tag{13}$$

2.2.4. Passive damping force model

The passive damping force $F_{passive}$ can be calculated by analyzing the pressure drop mechanism of the energy harvesting module without external load, hydraulic pipe, check valves and accumulator.

(1) Pressure drop of energy harvesting module without external load

Based on Eq. (7), when $R_{ex} = +\infty$, the relationship between pressure drop $\Delta P_{motor,passive}$ and volumetric flow rate Q_{motor} of the idling motor can be expressed as:

$$\Delta P_{motor,passive} = \frac{4\pi^2 J_g \eta_v}{q^2 \eta_m}\dot{Q}_{motor} = c_{motor,passive}\dot{Q}_{motor} \tag{14}$$

where $c_{motor,passive}$ is the equivalent passive damping coefficient of the energy harvesting module, which is subject to motor displacement, volumetric efficiency, mechanical efficiency and the moment of inertia of the generator rotor.

(2) Pressure drop of hydraulic pipe

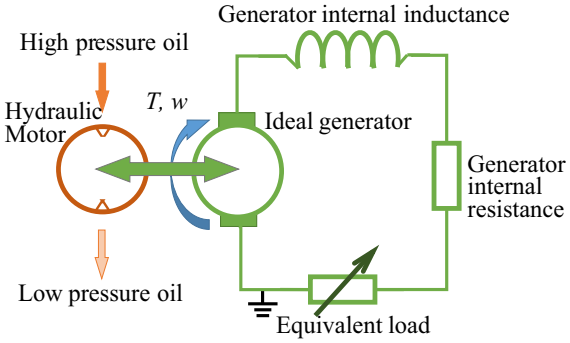

Fig. 7. Equivalent controllable damping force model.

When the damping oil flows through the external hydraulic pipe, the pressure drop ΔP_{pipe} can be approximated as:

$$\Delta P_{pipe} = \frac{128 L_{pipe}\mu}{\pi d_{pipe}^4} Q_{pipe} = k_{pipe} Q_{pipe} \tag{15}$$

where k_{pipe} is the pipe frictional pressure drop coefficient, Q_{pipe} is the volumetric flow rate (mm^3/s) through the pipe, L_{pipe} and d_{pipe} are the length (mm) and diameter (mm) of the pipe, respectively; μ is the dynamic viscosity ($N{\cdot}s/m^2$) of the damping oil.

(3) Pressure drop of the check valves

The two check valves in this scheme are all disc valve supported by coil spring, which can be set to a relatively low opening valve pressure and decreased passive damping. The orifice of the check valve is equivalent to a thin-wall hole, therefore, the relationship between the working pressure and pressure drop of the check valves can be expressed as:

$$Q_{valve\_i} = C_d A_{open\_i} U_{valve\_i} = C_d A_{open\_i} \sqrt{\frac{2\Delta P_{valve\_i}}{\rho}} \tag{16}$$

where Q_{valve_i}, A_{open_i}, U_{valve_i} and ΔP_{valve_i} are volumetric flow rate (mm^3/s), opening area (mm^2), flow velocity (mm/s) and pressure drop (Pa) of check valve i, $i = 1, 2$, respectively; C_d and ρ are the discharge coefficient and density (kg/mm^3) of the damping oil, respectively.

The opening area A_{open_i} in Eq. (16) also depends on pressure drop ΔP_{valve_i}. Assuming basic linearity for simplicity, for a valve lift X and exit width B, the calve exit area is $A = BX$, and the lift is $X = F/K$, the force is $F = A\Delta P$. With a leak area A_{leak_i}, the total valve exit area (A_{open_i}) of check valve i is then:

$$A_{open\_i} = \frac{B_{valve\_i} A_{valve\_i} \Delta P_{valve\_i}}{K_{valve\_i}} + A_{leak\_i} \tag{17}$$

where B_{valve_i}, A_{valve_i} and K_{valve_i} are exit width (mm), area (mm^2) and stiffness (N/mm) of the disc of vavle i, respectively, $B_{valve\_i} = \pi d_{valve\_i}$, d_{valve_i} is the diameter (mm) of the disc.By solving Eqs. (16) and (17) and neglecting the leak area A_{leak_i}, the pressure drop of valve i is:

$$\Delta P_{valve\_i} = \left(\sqrt{\frac{\rho}{2}} \frac{K_{valve\_i}}{C_d B_{valve\_i} A_{valve\_i}} Q_{valve\_i} \right)^{\frac{2}{3}} \tag{18}$$

(4) Pressure analysis of accumulator

The high-pressure nitrogen cavity can be equivalent to a gas diaphragm accumulator, which can use the expression/expansion of the gas to absorb/release oil pressure. Due to the fixed gas mass, the relationship between gas volume and gas pressure can be obtained by following ideal gas property:

$$P_0 V_0^n = P_t V_t^n \tag{19}$$

where P_0 and V_0 are the initial state gas pressure and volume in the accumulator, P_t and V_t are the gas pressure and volume at time t, respectively; n is polytropic exponent. Therefore, the relationship between V_t andV_0 is:

$$V_t - V_0 = A_r \int v(t) \mathrm{d}t \tag{20}$$

where A_r and $v(t)$ are the section area and velocity of piston rod, respectively.Solving Eqs. (19) and (20), P_t can be written as:

$$P_t = \frac{P_0 V_0^n}{V_t^n} = \frac{P_0 V_0^n}{\left(A_r \int v(t)\mathrm{d}t + V_0\right)^n} \tag{21}$$

The pressure of upper cavity ($P_{up,passive}$) and lower cavity ($P_{down,passive}$) of the piston can be calculated based on Fig. 5 and above Equations:

$$\begin{cases} P_{up,passive} = \Delta P_{motor,passive} + P_t + \Delta P_{pipe} \\ P_{down,passive} = P_t - \Delta P_{valve\_2} \end{cases}, \quad v(t) \geqslant 0 \tag{22}$$

$$\begin{cases} P_{up,passive} = \Delta P_{motor,passive} + P_t + \Delta P_{pipe} \\ P_{down,passive} = \Delta P_{motor,passive} + P_t + \Delta P_{pipe} + \Delta P_{valve\_1} \end{cases}, \quad v(t) \leqslant 0 \tag{23}$$

The total passive damping force $F_{passive}$ can be calculated using Eqs. (1), (2), (22) and (23):

$$\begin{aligned} F_{passive} &= A_c P_{up,passive} - A_g P_{down,passive} \\ &= \begin{cases} A_c(\Delta P_{motor,passive} + P_t + \Delta P_{pipe}) \\ \quad -A_g(P_t - \Delta P_{valve\_2}), \quad v(t) \geqslant 0 \\ A_c(\Delta P_{motor,passive} + P_t + \Delta P_{pipe}) \\ \quad -A_g(\Delta P_{motor,passive} + P_t + \Delta P_{pipe} + \Delta P_{valve\_1}), \quad v(t) \leqslant 0 \end{cases} \end{aligned} \tag{24}$$

2.2.5. Overall model

Finally, the total damping force F can be written as:

$$F = F_{semi-active} + F_{passive} \tag{25}$$

2.2.6. Parameter setup

After modeling this damper, a medium off-road vehicle is chosen to design its outline dimensions and connection structures. The parameters used to calculate the controllable and passive damping forces are listed in Table 1, in which, the external load is adjustable, the motor displacement and piston rod diameter are optimized by the authors' previous research [27,28].

3. Prototype design and test setup

3.1. Prototype design

Based on above design and modeling process, a regenerative damper prototype is designed and manufactured. This prototype will be used in the following experimental tests.

Table 1
Parameters used to calculate the controllable and passive damping forces.

	Parameters	Symbol	Valve	Unit
Generator	EMF constant	k_e	0.137	Vs/rad
	Torque constant	k_t	0.137	Vs/rad
	Internal resistance	R_{in}	0.08	Ω
	External load	R_{ex}	Adjustable	Ω
Pump	Volumetric efficiency	η_v	0.92	–
	Mechanical efficiency	η_m	0.95	–
	Displacement	q	6	cc
Actuator	Piston diameter	D	32.2	mm
	Piston rod diameter	d_{rod}	18	mm
Hydraulic pipe	Length	L_{pipe}	1400	mm
	Diameter	d_{pipe}	10	mm
Check valve 1	Disc diameter	d_{valve_1}	28	mm
	Disc stiffness	K_{valve_1}	750	N/mm
Check valve 2	Disc diameter	d_{valve_2}	24	mm
	Disc stiffness	K_{valve_2}	880	N/mm
Accumulator	Initial pressure	P_0	0.3	MPa
	Initial volume	V_0	67400	mm^3
	Polytropic exponent	n	1.4	–
Damping oil	Dynamic viscosity*	μ	1.24×10^{-2}	$N{\cdot}s/m^2$
	Density*	ρ	8.50×10^{-7}	kg/mm^3
	Discharge coefficient	C_d	0.7	–

Fig. 8. Actuator prototype of the pumping regenerative damper.

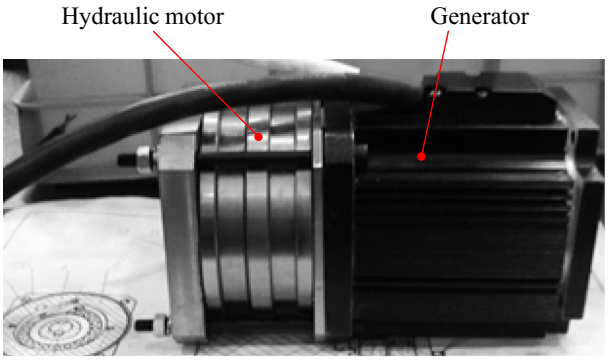

Fig. 9. Prototype of the energy harvesting module.

The actuator prototype is shown in Fig. 8, in which, the inflatable nuzzle is used to inject high pressure nitrogen into the reserve cavity and adjust the gas pressure. The oil outlet and inlet are connected to motor inlet and outlet via oil pipe, respectively. At the two ends of the actuator, two hoisting rings are used to facilitate the clamping and assembly in the following test.

The energy harvesting module prototype is shown in Fig. 9, in which, a brushless DC motor (Model: 80BL89S50-445) was chosen as the generator. In order to improve the integration of the whole system, a compact cycloid hydraulic motor was designed and manufactured to match with the generator.

The output of above generator is three-phase alternating current which cannot be directly stored in the battery pack. Therefore, the charge management module includes a three-phase rectifier to switch it into DC. Furthermore, a DC/DC buck-boost circuit is used to smooth the fluctuating voltage. The charge management module based LTC4000 controller (Linear Technology) is shown in Fig. 10, this module can stabilize the voltage and charge the 12 V battery effectively.

3.2. Test setup

In order to deeply explore the damping and regenerative characteristics of above prototype, we need to detect the signals of the actuator damping force, oil state, and the characteristics of the energy harvesting module. Therefore, a test system of the pumping regenerative damper is designed and built, as shown in Fig. 11. It mainly includes a high-speed EM shaker, a sensing system, and a control system, etc. Some key technical parameters and hardware models are shown in Table 2. The final manufactured test rig is shown in Fig. 12.

4. Results and discussions

4.1. Damping and temperature-rise characteristics under no-load mode

First of all, the passive damping characteristic under no-load mode (the external load is open circuit) was studied under both simulation and experimental tests. The damping characteristic shown in Fig. 13 is under the excitation of amplitude 50 mm and maximum frequency 1.655 Hz. The results show that, when the external load is open circuit, the maximum passive rebound/compression damping force under experimental test reach to 208 N/−235 N, they are all bigger than simulation valves. This is because that several sensors were mounted into the damping oil circuit, which could block the oil flow to some extent. Therefore, in the following energy harvesting characteristic tests, these sensors were removed to reduce the energy loss.

From the *F-v* curves shown in Fig. 13(b), we can see that the test speed curve has a more obvious valve-open point than the simulation curve. The cause is that the check valves in the actuator still have a relatively high valve-open pressure, this is also another reason for that the test damping forces are bigger that the simulation ones. Although there is still some passive damping in this regenerative damping, it is much smaller than the conventional dampers due to the novel oil circuit design. What's more, the damping oil flow is leaded out of the actuator and formed a large unidirectional oil flow cycle, which will improve the spread ability of the oil heat. These properties of this design will result in a small temperature-rise of the damping oil. The temperature of the damping oil

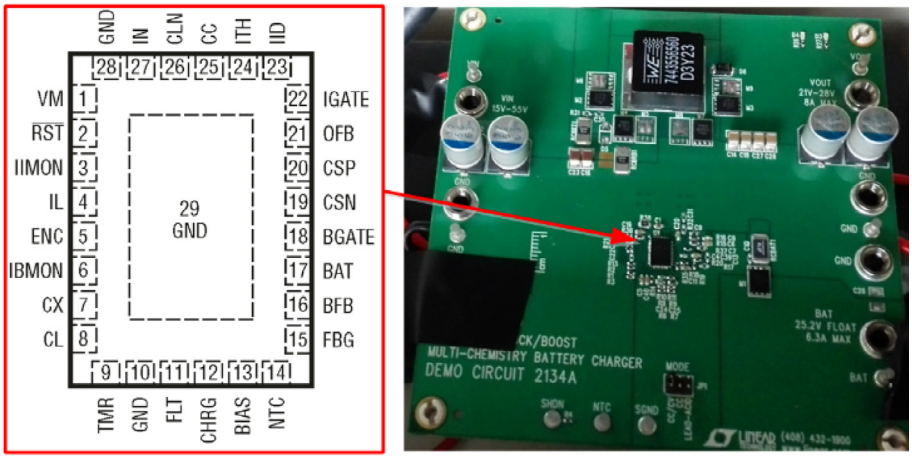

Fig. 10. Charge management module based on LTC4000. (a) LTC4000, (b) hardware.

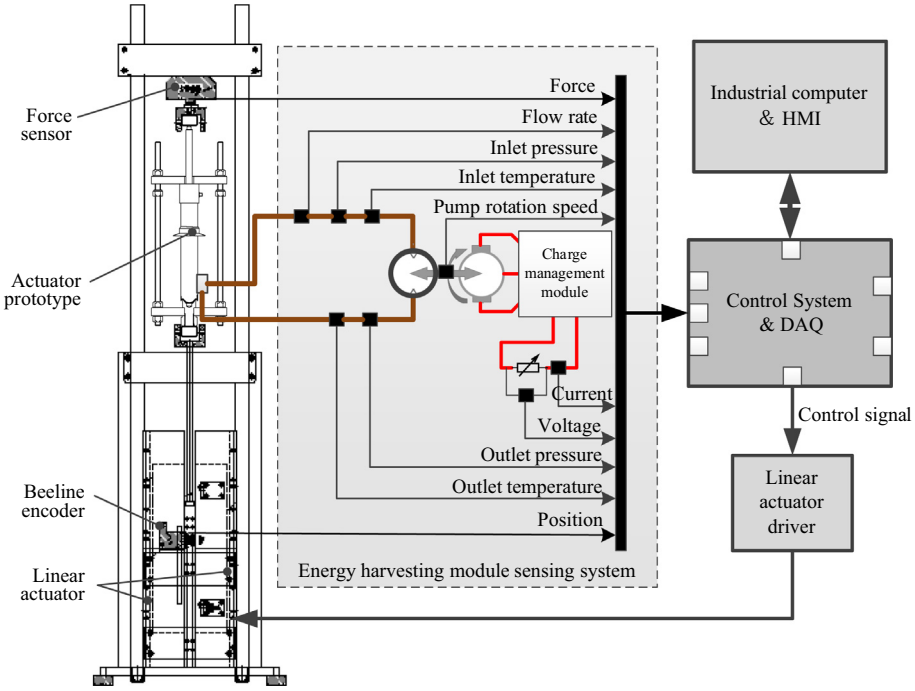

Fig. 11. Test system of the pumping regenerative damper.

Table 2
Key technical parameters and hardware model of the test rig.

Parameters	Valve	Unit	Hardware model	Accuracy
Stroke	0.25–200	mm	Position sensor (RENISHAW)	1 μm
Maximum excitation frequency	100	Hz	Force sensor (Interface1210AF)	0.04%
Peak operating force	8500	N	Linear actuator (Aerotech BLMX-502)	–
Peak operating speed	3	m/s	U-shape sliding guide (Aerotech MTX480)	–

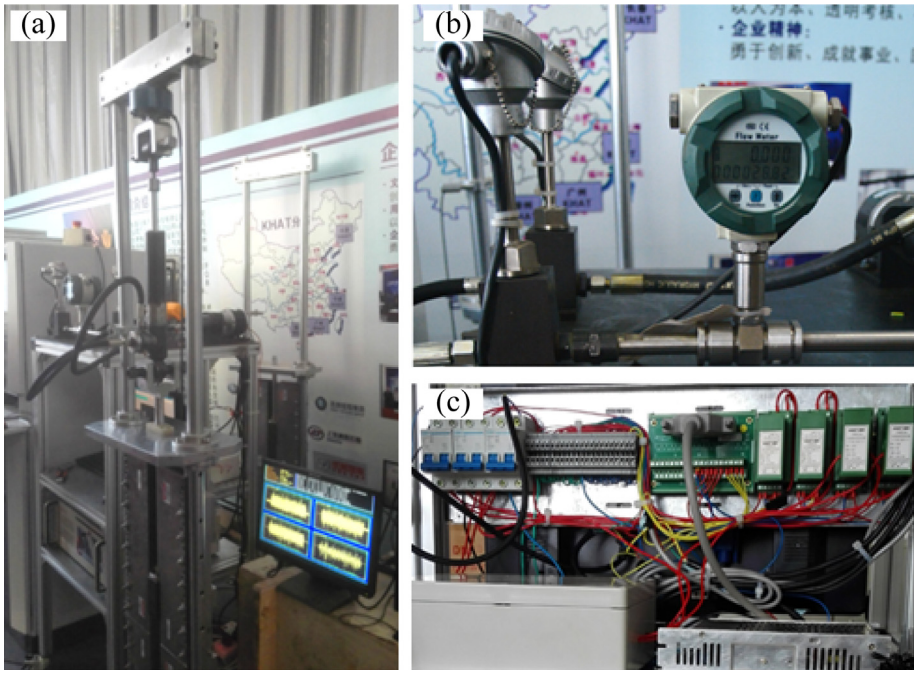

Fig. 12. Key parts of the test system. (a) Test system, (b) oil parameters related sensors, and (c) electrical parameters related sensors and electrical system.

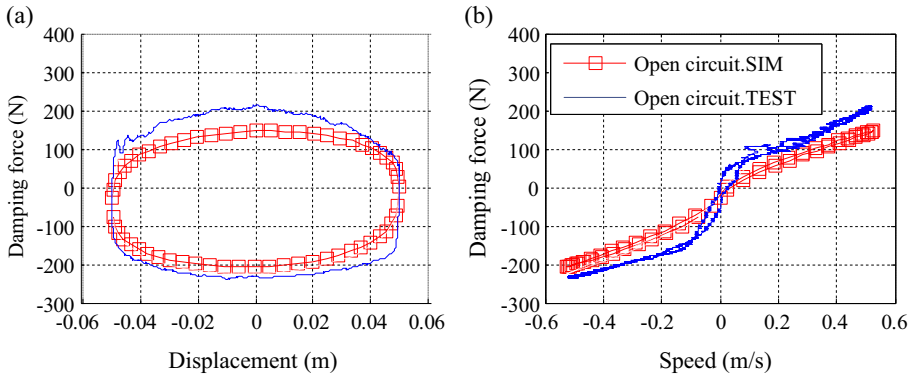

Fig. 13. Simulation and test results of damping characteristic under open circuit. (a) *F-s* curves, (b) *F-v* curves.

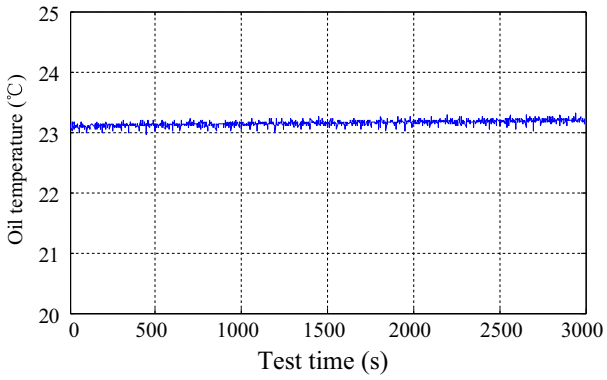

Fig. 14. Test result of temperature-rise characteristic under open circuit.

acquired from the test is shown in Fig. 14, the result shows that the temperature-rise is very slight during the test.

4.2. Damping controllable characteristic

From theoretical modeling processes, we can see that the damping force depends on both excitation frequency and external load. With a same amplitude, the excitation frequency is proportional to excitation speed. Therefore, the same amplitude 50 mm and different speeds and external loads were chosen to study the damping controllable range of this regenerative damper. The test setup is shown in Table 3.

With the maximum excitation speed 0.13 m/s and different external loads (10 Ω, 30 Ω, 60 Ω, 100 Ω), the damping characteristic is shown in Fig. 15. The maximum rebound force ranges from 489 N to 1236 N, and the adjustable multiple is 2.5. However, the compression force range is much smaller: −333 to −265 N, and the adjustable multiple is only about 1.26. This is mainly because the damping oil volumetric flow rate through the motor is relatively small during the compression stroke, which results in the low rotation speed of the motor and weak effect of the generator EMF. Therefore, the damping force is mainly provided by the passive damping of the hydraulic circuit but not the controllable one.

With the maximum excitation speed 0.26 m/s, the damping characteristic is shown in Fig. 16. The maximum rebound force ranges from 529 N to 2720 N and the adjustable multiple is 5.14, which is much bigger than the one when maximum speed is 0.13 m/s. Moreover, the compression force range also increases to 2.23.

With the maximum excitation speed 0.52 m/s, the damping characteristic is shown in Fig. 17. The maximum rebound/

Table 3
Test setup under different excitement speeds and external loads.

Parameters	Valve				Unit
External load	10	30	60	100	Ω
Amplitude	±50				mm
Maximum excitation speed	0.13	0.26	0.52		m/s
Maximum excitation frequency	0.414	0.828	1.655		Hz

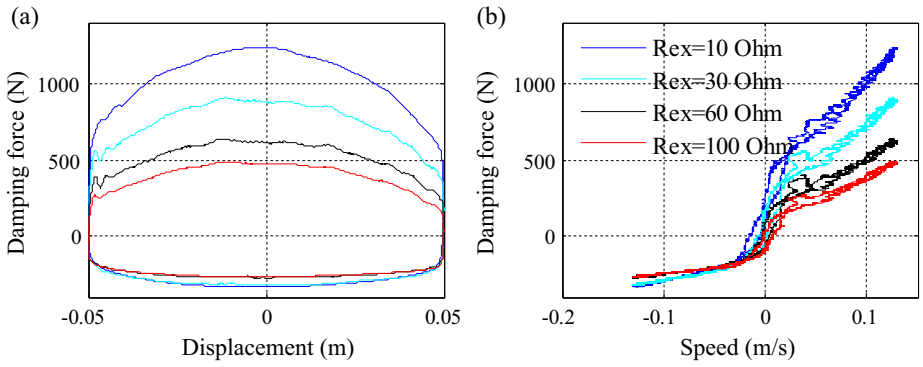

Fig. 15. Damping characteristic under maximum speed 0.13 m/s and different external loads. (a) *F-s* curves, (b) *F-v* curves.

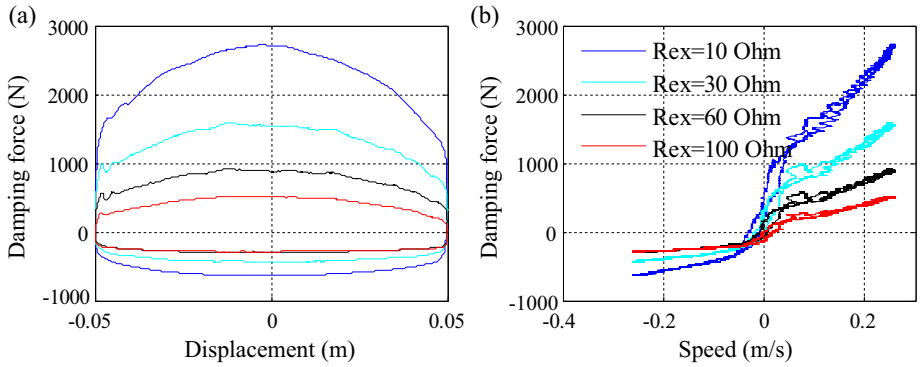

Fig. 16. Damping characteristic under maximum speed 0.26 m/s and different external loads. (a) *F-s* curves, (b) *F-v* curves.

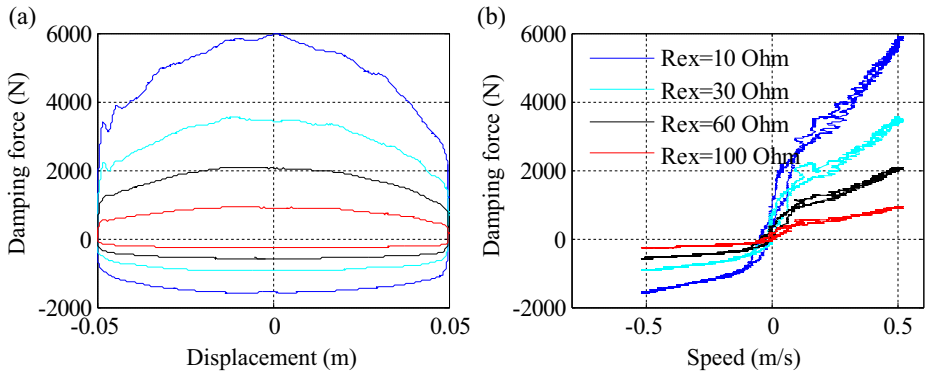

Fig. 17. Damping characteristic under maximum speed 0.52 m/s and different external loads. (a) *F-s* curves, (b) *F-v* curves.

compression force ranges all further increase to larger ones, 928–5966 N. N ~ 5966N and 6.43 for rebound, and −1599 to −367 N and 4.36 for compression. These valves are suitable for semi-active suspension control of medium off-road vehicles and some military vehicles.

It should be noted that the external load can be further decreased to less than 10 Ω, which will make the damper provide enlarged rebound/compression force ranges and adjustable multiples. But considering the power limitation of the external load and the bearing capacity of the energy harvesting module, we did not carry out these tests.

4.3. Regenerative characteristic

With the same test setup shown in Table 3, the output voltage and current signals of the charge management module were collected by the sensing system, then the regenerative output power of this prototype was calculated, as shown in Figs. 18 and 19.Fig. 18 shows the output power curves under the same maximum excitation speed 0.52 m/s and different external loads, it is consistent with the simulation result. The output power increases as the external load decreases. When the external load is 10 Ω, the peak output power reaches about 200 W, and the average is 110.6 W. However, the output power drops dramatically when the load increases, the average powers for 30 Ω, 60 Ω and 100 Ω are 66.4 W, 20.4 W and 9.6 W, respectively.

With the maximum speed 0.26 m/s, the output power curves are shown in Fig. 19. The results show that the power is relatively low, and the average powers for different external loads (10 Ω, 30 Ω, 60 Ω, 100 Ω) are 31.6 W, 19.0 W, 5.6 W and 3.0 W, respectively. One of the fundamental reasons is that the volumetric flow rate through the motor is low, leading to a reduced rotation speed

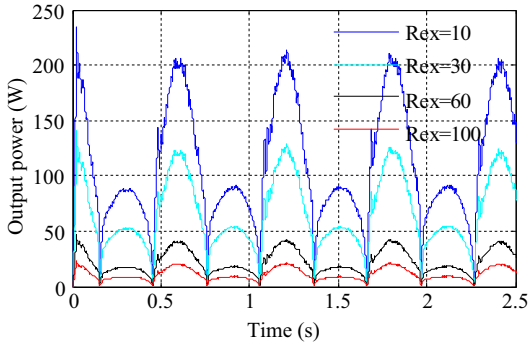

Fig. 18. Regenerative characteristic under maximum speed 0.52 m/s and different external loads.

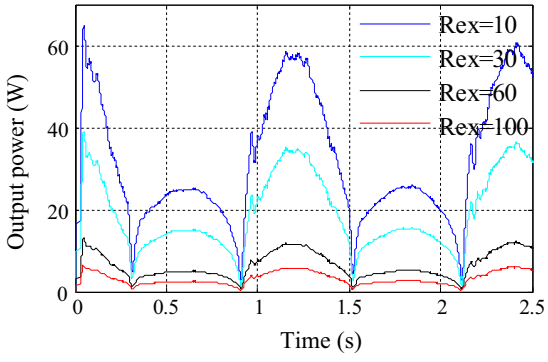

Fig. 19. Regenerative characteristic under maximum speed 0.26 m/s and different external loads.

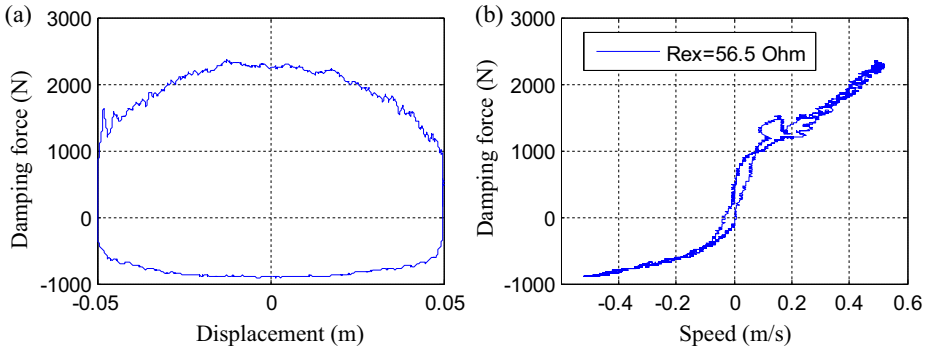

Fig. 20. Damping characteristic under target external load. (a) *F-s* curves, (b) *F-v* curves.

of the generator, which is much smaller than its nominal speed, and finally makes the generating efficiency of the generator decrease sharply.

4.4. Target damping characteristic

According to the suspension requirement of the target off-road vehicle, the rebound/compression damping forces should be close to 2200 N/−900 N under the standard excitation (maximum frequency 1.655 Hz and amplitude 50 mm). In order to obtain the external load which can provide these target damping forces, a series various external loads bench tests were conducted. Finally, the target damping characteristic shown in Fig. 20 was obtained under external load 56.5 Ω. The maximum rebound/compression damping forces are 2195 N/−916 N., basically meeting the requirement of the target off-road vehicle suspension. Therefore, the external load 56.5 Ω can be used when the suspension works in the passive mode.

5. Conclusions

This paper proposed an electro-hydraulic energy harvesting damper for off-road vehicles. Its design requirements and mathematical model were introduced in details, and a prototyping damper was designed and manufactured to experimentally validate its damping and energy regenerative characteristics. The main conclusions include:

(1) The designed regenerative damper meets these three design requirements well, namely unidirectional generator rotation, asymmetry rebound/compression damping force, and relatively large controllable range of damping force;
(2) The controllable range of damping force depends on excitation intensity and external load valve. It is much bigger under severe input and small load; this property is a basis to design the energy harvesting active or semi-active suspension control system;
(3) The regenerative power also depends on the excitation intensity and external load valve. With maximum excitation speed 0.52 m/s and external load 10 Ω, the peak output power reaches about 200 W, and the average is 110.6 W. The results also show a trade-off between energy harvesting and damping characteristic.

The developed electro-hydraulic energy harvesting damper provides a good option to harvest energy and improve fuel efficiency of off-road vehicles. Future issues include: (1) coupling mechanism study of the regenerative suspension and vehicle driving performances, (2) dual-mode control algorithm design to better balance the damping and regenerative characteristics, and (3) adaption design of the suspension energy flow and the powertrain system energy flow of the vehicles.

Acknowledgements

This work is supported in part by the National Nature Science Foundation of China (No. 61520106008 and No. 61522307) and the High Technology Research and Development Program of Jilin, China (No. 20130204021GX). We would like to gratefully acknowledge and thank KH Automotive Technologies, which funded the test bench and prototype design in this project. Special thanks to Prof. Karl Hedrick of UC Berkeley, and Dr. Dai Wang of Lawrence Berkeley National Lab, for their helpful discussions and suggestions on this research topic.

References

[1] Ruan J, Walker P, Zhang N. A comparative study energy consumption and costs of battery electric vehicle transmissions. Appl Energy 2016;165:119–34.
[2] Fiori C, Ahn K, Rakha HA. Power-based electric vehicle energy consumption model: model development and validation. Appl Energy 2016;168:257–68.
[3] Rauh J, Ammon D. System dynamics of electrified vehicles: some facts, thoughts, and challenges. Vehicle Syst Dynam 2011;49(7):1005–20.
[4] Crolla DA, Cao D. The impact of hybrid and electric powertrains on vehicle dynamics, control systems and energy regeneration. Vehicle Syst Dynam 2012;50(S1):95–109.
[5] Chung CT, Hung YH. Performance and energy management of a novel full hybrid electric powertrain system. Energy 2015;89:626–36.
[6] Li L, Li X, Wang X, Song J. Analysis of downshift's improvement to energy efficiency of an electric vehicle during regenerative braking. Appl Energy 2016;176:125–37.
[7] Xie XD, Wang Q. Energy harvesting from a vehicle suspension system. Energy 2015;86:385–92.
[8] US Department of Energy. Energy efficiency & renewable energy, where the energy goes: gasoline vehicles [DB/OL]; 2016. <http://www.fueleconomy.gov/feg/atv.shtml>.
[9] Zhang Y, Guo K, Wang D, et al. Energy conversion mechanism and regenerative potential of vehicle suspensions. Energy 2017;119:961–70.
[10] Zuo L, Zhang PS. Energy harvesting, ride comfort, and road handling of regenerative vehicle suspensions. J Vib Acoust 2011;135(1):48–65.
[11] Audi's latest chassis suspension system innovation: eROT (electromechanical rotary damper) [DB/OL]; 2016. <http://www.audi.com/corporate/en/innovations.html>.
[12] Els PS, Theron NJ, Uys PE, et al. The ride comfort vs. handling compromise for off-road vehicles. J Terrramech 2007;44(4):303–17.
[13] Crolla DA, Abouel Nour AMA. Power losses in active and passive suspensions of off-road vehicles. J Terrramech 1992;29(1):83–93.
[14] Zuo L, Scully B, Shestani J, Zhou Y. Design and characterization of an electromagnetic energy harvester for vehicle suspensions. Smart Mater Struct 2010;19(4):045003.
[15] Song X, Li Z, Edmondson JR. Regenerative passive and semi-active suspension. U.S. Patent No. 7,087,342; Aug 8, 2006.
[16] Kawamoto Y, Suda Y, Inoue H, Kondo T. Electro-mechanical suspension system considering energy consumption and vehicle maneuver. Vehicle Syst Dynam 2008;46(S1):1053–63.
[17] Singal K, Rajamani R. Zero-energy active suspension system for automobiles with adaptive sky-hook damping. J Vib Acoust 2013;135(1):011011.

[18] Li Z, Zuo L, Luhrs G, Lin L, Qin Y. Electromagnetic energy-harvesting shock absorbers design, modeling and road tests. IEEE Trans Veh Technol 2013;62(3):1065–75.
[19] Li Z, Zuo L, Kuang J, Luhrs G. Energy-harvesting shock absorber with a mechanical motion rectifier. Smart Mater Struct 2013;22(2):025008.
[20] Zhang Z, Zhang X, Chen W, et al. A high-efficiency energy regenerative shock absorber using supercapacitors for renewable energy applications in range extended electric vehicle. Appl Energy 2016;178:177–88.
[21] Choi SB, Seong MS, Kim KS. Vibration control of an electrorheological fluid-based suspension system with an energy regenerative mechanism. Proc Inst Mech Eng, Part D: J Autom Eng 2009;223(4):459–69.
[22] Sapiński B. Vibration power generator for a linear MR damper. Smart Mater Struct 2010;19(10):105012.
[23] Sapiński B. Experimental study of a self-powered and sensing MR-damper-based vibration control system. Smart Mater Struct 2011;20(10):105007.
[24] Stansbury III, James A. Regenerative suspension with accumulator systems and methods. U.S. Patent No. 20,120,313,575; Dec 13, 2012.
[25] Guo K, Zhang Y, Chen Y, et al. Pumping energy harvesting active damping system. China Patent No. CN203463546U; Dec. 25, 2013.
[26] Guo K, Zhang Y, Zhen H, et al. Pumping energy harvesting interconnected suspension system. China Patent No. CN104154165A; Nov. 19, 2014.
[27] Zhang Y, Zhang X, Zhan M, et al. Study on a novel hydraulic pumping regenerative suspension for vehicles. J Franklin Inst 2014;352(2):485–99.
[28] Zhang Y, Guo K, Zhang X, et al. Energy harvesting piston assembly and shock absorber. China Patent No. CN105782320A; Jul. 20, 2016.